

# Zero-Current Phenomena Analysis of the Single IGBT Open Circuit Faults in Two-Level and Three-Level SVGs

Ke Wang<sup>†</sup>, Hong-Lu Zhao<sup>\*</sup>, Yi Tang<sup>\*</sup>, Xiao Zhang<sup>\*</sup>, and Chuan-Jin Zhang<sup>\*</sup>

<sup>†,\*</sup>School of Electrical and Power Engineering, China University of Mining and Technology, Xuzhou, China

## Abstract

The fact that the reliability of IGBTs has become a more and more significant aspect of power converters has resulted in an increase in the research on the open circuit (OC) fault location of IGBTs. When an OC fault occurs, a zero-current phenomena exists and frequently appears, which can be found in a lot of the existing literature. In fact, fault variables have a very high correlation with the zero-current interval. In some cases, zero-current interval actually decides the most significant fault feature. However, very few of the previous studies really explain or prove the zero-current phenomena of the fault current. In this paper, the zero-current phenomena is explained and verified through mathematical derivation, based on two-level and three-level NPC static var generators (SVGs). Mathematical models of single OC fault are deduced and it is concluded that a zero-current interval with a certain length follows the OC faults for both two-level and NPC three-level SVGs. Both inductive and capacitive reactive power situations are considered. The unbalanced load situation is discussed. In addition, simulation and experimental results are presented to verify the correctness of the theoretical analysis.

**Key words:** Fault diagnosis, IGBT OC fault, NPC 3-Level, SVG, 2-level, Zero-current

## I. INTRODUCTION

The IGBT, as one of the most successful power switching devices, is widely used in converter applications. IGBTs normally operate at a high switching frequency and have a high stability requirement [1]. Once a semiconductor device fails, the system is damaged, which results in serious losses.

Short-circuit (SC) and open-circuit (OC) faults are the two most common faults for IGBTs. When compared with SC faults [2], which are usually destructive and result in a direct shut down of the system, OC faults are more likely to go undetected, but significantly reduce the system performance. In order to reduce the impact of an OC fault on the system, many studies have been done [3], [4]. They mainly include two aspects: fault location and fault tolerance.

The goal of fault location is to lock OC faulty IGBT with

minimal time, minimum cost, and maximum stability. Generally speaking, current-based and voltage-based methods are the two most common OC fault diagnosis strategies.

A number of current-based proposals have been presented in the literature. The current Park's Vector method was proposed in [5], [6]. However, it requires very complex pattern recognition algorithms, which are not suitable for integration into drive controllers. The average current Park's Vector method was proposed in [7]. Methods based on an analysis of the current space vector trajectory diameter were discussed in [8], [9]. To overcome the defects of load dependence and sensitivity to transients, a normalized average current method was proposed in [10], and the absolute values of the normalized average currents were considered in [11]. A combined method based on both a derivative of the current Park's vector phase and the current polarity was proposed in [12]. It possesses excellent immunity to false alarms. Current-based methods are independent of system parameters and no additional sensors are needed. However, the corresponding diagnostic time is generally longer than a supply period.

Voltage-based methods have a faster response than current-based methods [13], [14]. However, they usually need additional

Manuscript received May 23, 2017; accepted Nov. 4, 2017

Recommended for publication by Associate Editor Kyo-Beum Lee.

<sup>†</sup>Corresponding Author: kewang\_china@cumt.edu.cn

Tel: +86-13952171593, China Univ. of Mining and Tech.

<sup>\*</sup>School of Electrical and Power Eng., China Univ. of Mining and Tech., China

detection hardware, which increases the drive costs and complexity. A direct comparison between the measured voltages and the reference values was presented in [15] and a time delay was introduced to prevent false alarms. A FPGA based fault location approach with detection times shorter than 10  $\mu$ s was introduced in [16]. Alternatively, a low-cost proposal based on indirect voltage measurement using high-speed photocouplers was presented in [17]. However, well-defined time delays dependent on the nature of the power converter are still required.

In addition, some other methods, such as the wave-let fuzzy algorithm [18], wavelet-neural network [19] and rule-based expert systems [20] can also be used for OC fault diagnosis. For expert systems, user input can be a combination of system parameters, such as three phase currents, inverter pole voltage, phase voltage, switch voltages, DC link current and user inputs.

The goal of fault tolerance is to ensure that a system continues to operate and maintain a good performance through software and hardware strategies before an open-circuit fault is repaired. Fault tolerance consists of fault isolation and fault reconfiguration, which is based on hardware redundancy and fault-tolerant control.

Previous studies provide a large number of methods for fault redundancy. These methods can be classified into four categories: switch-level, leg-level, module-level and system-level. For switch-level solutions, inherently redundant switching states methods [21], dc-bus midpoint installation methods [22] and redundant parallel or series switch installation methods [23] are proposed. In leg-level solutions, the main approach is to add redundant legs in parallel or series connection to the main legs [24]. When choosing redundant parallel methods, a compromise between system cost and performance must be considered.

In terms of the OC fault diagnosis and tolerance for converters in the literature, when focusing on the existing designs for two-level or three-level converters, it can be found that a zero current phenomena exists and frequently appears in the OC fault condition. When an OC fault occurs, the fault phase current is greatly distorted, through random increases and decreases. The fault phase current can even drop to zero in some cases and stay there for a period of time. This phenomena can be found in many of the existing studies [17], [25]-[29], regardless of whether they are designed for motor drive applications or grid connected inverters.

The zero current phenomena should be taken seriously. Meanwhile, almost all of the existing papers just focus on how to locate OC faults and very few of them value the importance of the zero current. In fact, many of the fault variables presented in existing papers have a great correlation with the zero-current interval. In some cases, the zero-current interval actually decides the most significant fault feature. For example, for the excellent average current method in [10], the proposed decision function is greatly increase in the

zero-current interval. In [28], a good strategy for OC fault detection is proposed based on the average current Park's vector method. If the zero current phenomena occurs or the current values are close to zero, the average line current vector greatly increases and becomes higher than the threshold. In [29], the diagnostic variables  $d_n$  and  $a_n$  are also greatly determined, since  $\langle |i_n| \rangle$  is close to zero in the zero-current interval. By observing many of the fault current waveforms in the literature, it is worth noting that all of the results of multiplication involved with the fault phase current  $i$  are zero when it comes to the zero-current interval, such as:

$$\int_{t_0}^{t_1} i \cdot dt = \int_{t_0}^{t_1} i^2 \cdot dt = \int_{t_0}^{t_1} (u \cdot i) \cdot dt = 0 \quad (\text{when } i=0 \text{ for } t_0 < t < t_1).$$

For OC fault diagnosis, especially for current-based OC fault location, the zero-current interval corresponds to the most significant fault feature. This leads to a number of questions. Why does the zero current phenomena occur? When will zero current occur? And how long will the zero current phenomena last? Therefore, learning the rules of the zero current in an OC fault is meaningful and important to the understanding of OC faults and OC fault location methods.

Some studies discussed how the fault current changes after an OC fault such as in two-level converters [27], [30]-[32] and in three-level converters [33]-[40]. However no existing papers have really explained the zero-current phenomena.

The innovations in this paper are as follows:

- Zero-current phenomena is explained and verified through mathematical derivations based on two-level and three-level NPC SVG.
- It is concluded that the zero-current phenomena must occur after an IGBT OC fault as long as the converters work under the pure reactive power condition. It is verified that a zero-current interval with a certain length follows OC faults for both two-level and NPC three-level SVGs as shown in Table III.
- Mathematical models of a single OC fault are given in this paper. Mathematical expressions of the fault phase current in a single OC fault are also presented.
- Both capacitive and inductive reactive power condition are considered. In addition, the unbalanced load condition is discussed.

In addition, a clear definition of the polluted-area and zero-current interval are given. Simulation and experimental results are presented to verify the correctness of the analysis. This analysis method also applies to other rectifier occasions.

This paper is organized as follows. In Section II, the zero-current after an OC fault is analyzed based on a two-level static var generator. Both inductive and capacitive reactive power situations are considered. Then, the zero-current after an OC fault is analyzed based on a NPC three-level static var generator in Section III. Similarly, both inductive and capacitive reactive power situations are considered. The

unbalanced load situation is discussed in Section IV. Experimental results are illustrated in Section V to verify the correctness of the simulations. Finally, some conclusions are summarized in Section VI.

## II. ZERO-CURRENT ANALYSIS OF AN OC FAULT IN A TWO-LEVEL SVG

The two-level SVG topology is represented in Fig. 1. For each leg ( $A$  or  $B$  or  $C$ ), there are two IGBTs and two Diodes, which are defined as  $S_{X1}$ ,  $S_{X2}$ ,  $D_{X1}$  and  $D_{X2}$ . In this paper,  $X \in (A, B, C)$ . The output current  $i_X$  of leg  $X$  is shown in Fig. 1, with a reference direction.

The pulse state is given by:

$$S_X = \begin{cases} 1 & S_{X1} = \text{on}, S_{X2} = \text{off} \\ 0 & S_{X1} = \text{off}, S_{X2} = \text{on} \end{cases} \quad (X \in A, B, C) \quad (1)$$

### A. Inductive Reactive Power Condition

Assuming that pure inductive reactive power is generated for a SVG system, the three phase current  $i_A$ ,  $i_B$  and  $i_C$  are fundamental sinusoidal shaped with 90 degrees delays of the grid voltages  $e_A$ ,  $e_B$  and  $e_C$ , respectively. If an OC fault occurs, the fault phase current is greatly distorted. A typical example of a  $S_{A1}$  OC fault in the inductive reactive power condition is introduced in Fig. 2, which shows  $i_A$  and  $e_A$  in both the normal and fault conditions. It can be seen that the positive half-cycle of the current  $i_A$  has been seriously affected.

As shown in Fig. 2, the area of  $i_A \geq 0$  (shadow area) is defined as the current-polluted area in a  $S_{A1}$  OC fault. The reason is as follows. If  $i_A < 0$ , regardless of whether  $S_A = 1$  or  $S_A = 0$ ,  $i_A$  does not flow through  $S_{A1}$ , which means that the failure of  $S_{A1}$  has no effect on the system. In the current-polluted area (area  $i_A \geq 0$ ) only, the current failed to flow through  $S_{A1}$  to the bus “+” under the condition of  $S_A = 1$ , resulting in the current distortion phenomena.

In addition, in the current-polluted area, the current does not flow through  $S_{A2}$  or  $D_{A1}$  due to the unidirectional conductance. Then,  $D_{A2}$  provides a unique current path for  $i_A$  unless phase  $A$  is isolated ( $i_A = 0$ ). Therefore, a system with a  $S_{A1}$  OC fault can be simplified as shown in Fig. 3.

Ignoring the on-state voltage drop of the IGBT and diode, the mathematical model of SVG in the current-polluted area can be expressed as (2)-(5):

$$V_{MN} = -S_B \cdot u_{dc} + i_B \cdot r_B + L_B \cdot \frac{di_B}{dt} + e_B \quad (2)$$

$$V_{MN} = -S_C \cdot u_{dc} + i_C \cdot r_C + L_C \cdot \frac{di_C}{dt} + e_C \quad (3)$$

$$V_{MN} = i_A \cdot r_A + L_A \cdot \frac{di_A}{dt} + e_A \quad (4)$$

$$i_A \geq 0 \text{ (} S_{A1} \text{ OC fault of a two-level SVG)} \quad (5)$$

Assuming that  $r_A = r_B = r_C = 0$ ,  $L_A = L_B = L_C$ ,  $i_A + i_B + i_C = 0$ ,  $\frac{di_A}{dt} + \frac{di_B}{dt} + \frac{di_C}{dt} = 0$  and  $e_A + e_B + e_C = 0$ , it can be deduced by

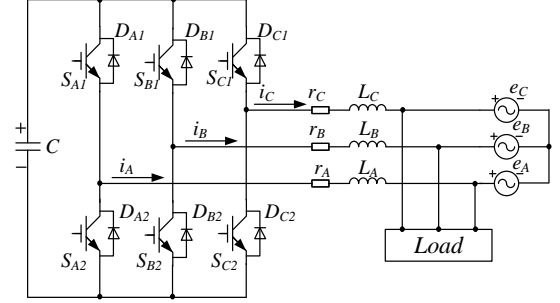


Fig. 1. Schematic of a two-level SVG.

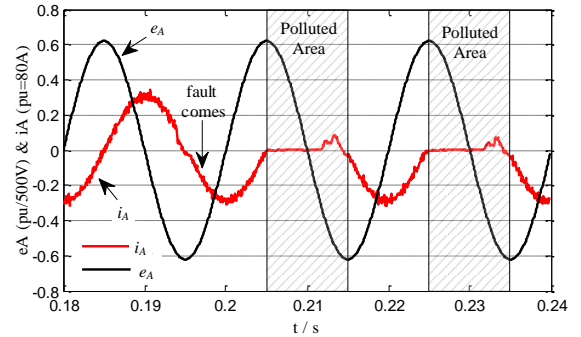


Fig. 2. Fault phase current  $i_A$  before and after a  $S_{A1}$  OC fault.

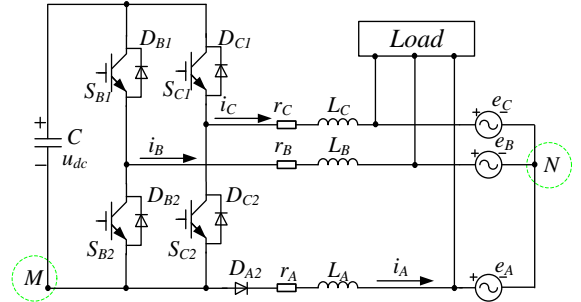


Fig. 3. Simplified schematic of a two-level SVG in a  $S_{A1}$  OC fault.

(2)-(5) that:

$$-L_A \cdot \frac{di_A}{dt} = \frac{1}{3}(S_B + S_C) \cdot u_{dc} + e_A \quad (i_A \geq 0) \quad (6)$$

As shown in (6), the sign of the current rate of change  $di_A/dt$  is determined by  $S_B$ ,  $S_C$ ,  $u_{dc}$  and  $e_A$ , among which  $u_{dc}$  can be considered as a stable constant, and  $e_A$  can be expressed as:

$$e_A = U_m \cdot \cos(\theta) \quad (7)$$

Let  $f = (S_B + S_C) \cdot u_{dc}/3$ . If  $S_B = S_C = 0$ , then  $f = 0$ . If  $S_B = 1, S_C = 0$  or if  $S_B = 0, S_C = 1$ , then  $f = u_{dc}/3$ . If  $S_B = 1, S_C = 1$ , then  $f = 2 \cdot u_{dc}/3$ . For a clearer explanation, the curves of  $e_A$  and  $-f$  are shown in Fig. 4(a). Assuming that  $1.7 \cdot U_m < u_{dc} < 3 \cdot U_m$ , which is usually employed for SVG applications, the intersections  $P$  of the curves are:  $P_1(\theta_1 = 90^\circ)$ ,  $P_2(\theta_2 = \arccos(-u_{dc}/(3 \cdot U_m)))$  and  $P_3(\theta_3 = 180^\circ)$ .

By comparing the values of  $e_A$  and  $-f$  in Fig. 4(a), the sign of  $di_A/dt$  in (6) is easily obtained, as follows:

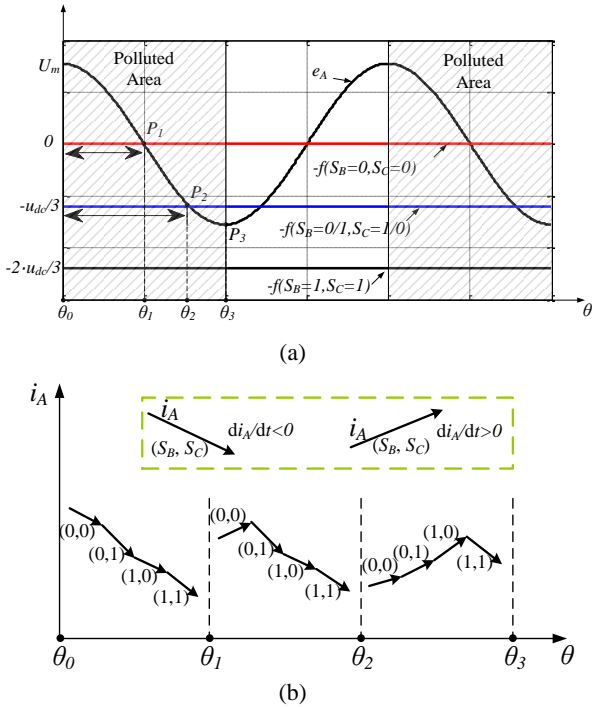


Fig. 4.  $S_{A1}$  OC fault in the inductive power condition for a two-level SVG: (a) comparison between  $e_A$  and  $-f$ ; (b) effect of  $(S_B, S_C)$  on the sign of  $di_A/dt$ .

In the interval  $\theta: (\theta_0 - \theta_1)$ , for the pulse states  $(S_B, S_C)$ ,  $di_A/dt < 0$ .

In the interval  $\theta: (\theta_1 - \theta_2)$ , for the pulse state  $(S_B=0, S_C=0)$ ,  $di_A/dt > 0$ ; and for the other three pulse states  $(S_B, S_C)$ ,  $di_A/dt < 0$ .

In the interval  $\theta: (\theta_2 - \theta_3)$ , for the pulse state  $(S_B=1, S_C=1)$ ,  $di_A/dt < 0$ ; and for the other three pulse states  $(S_B, S_C)$ ,  $di_A/dt > 0$ .

The effect of  $(S_B, S_C)$  on the sign of  $di_A/dt$  is displayed more vividly in Fig. 4(b), where it can be seen that the value of  $i_A$  keeps decreasing regardless of the states of  $(S_B, S_C)$  in the interval  $\theta: (\theta_0 - \theta_1)$ . Since  $i_A$  happens to pass through the zero point at  $\theta_0$ , the value of  $i_A$  must be zero in the interval  $\theta: (\theta_0 - \theta_1)$ . Then, the following conclusions can be drawn:

**Conclusion I:** When a  $S_{A1}$  OC fault occurs in a two-level SVG in the pure inductive reactive power condition, there must be a zero-current interval with a length of  $90^\circ$ , i.e. 1/4 of a supply period.

In addition, it can be seen that  $i_A$  is still difficult to establish in the interval  $\theta: (\theta_1 - \theta_2)$  of Fig. 4(b), because it is increased only when the pulse state is  $(S_B=0, S_C=0)$ . The fault phase current does not recover until it enters the interval  $\theta: (\theta_2 - \theta_3)$ .

To verify the validity of Conclusion I, a MATLAB / SIMULINK model has been built. The system parameters involved in the simulation are shown in Table I.

Simulation results of a  $S_{A1}$  OC fault are shown in Fig. 5. In Fig. 5(a),  $(\theta_0, \theta_1, \theta_2, \theta_3)$  are  $(0^\circ, 90^\circ, 140.5^\circ, 180^\circ)$ . The  $S_{A1}$  OC fault occurs in the negative half-cycle of the A-phase current. However,  $i_A$  is not polluted until it enters the current-polluted

TABLE I  
SIMULATION PARAMETERS

Parameter	Value
$e_{AB}, e_{BC}, e_{CA}$	380V(RMS)
$i_A, i_B, i_C$	28A(RMS)
$L_A, L_B, L_C$	1mH
$u_{dc}$	720V
Bus capacitance C	4800 $\mu$ F
Switching frequency	5kHz
Sampling frequency	12.5kHz

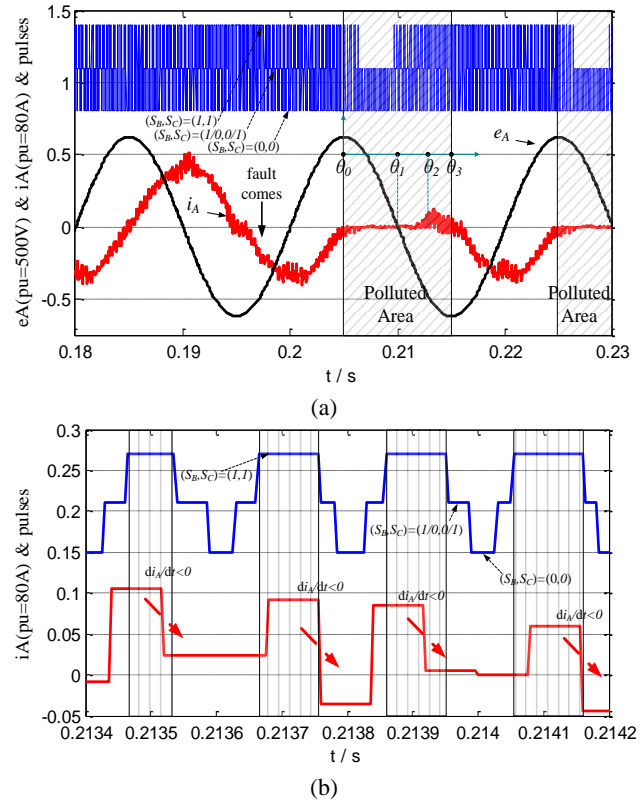


Fig. 5. Simulation results of a  $S_{A1}$  OC fault in the inductive power condition for a two-level SVG: (a) fault phase current  $i_A$ , supply voltage  $e_A$  and  $(S_B, S_C)$ ; (b)  $di_A/dt$  and  $(S_B, S_C)$ .

area. A zero-current interval with a length of  $90^\circ$  clearly exists in the interval  $\theta: (\theta_0 - \theta_1)$ . Then,  $i_A$  recovers in the interval  $\theta: (\theta_2 - \theta_3)$ . Fig. 5(b) shows details of both  $(S_B, S_C)$  and  $i_A$  in the interval  $\theta: (\theta_2 - \theta_3)$ , where  $i_A$  decreases right after the function of the pulse  $(S_B=1, S_C=1)$  and increases at the rest values of  $(S_B, S_C)$ . The simulation results verify the correctness of Conclusion I.

For a two-level SVG, this section explains only a  $S_{A1}$  OC fault. However, it is quite easy to introduce the other five IGBT OC faults with similar conclusions, and that a zero-current interval with a length of  $90^\circ$  must exist in the inductive reactive power condition.

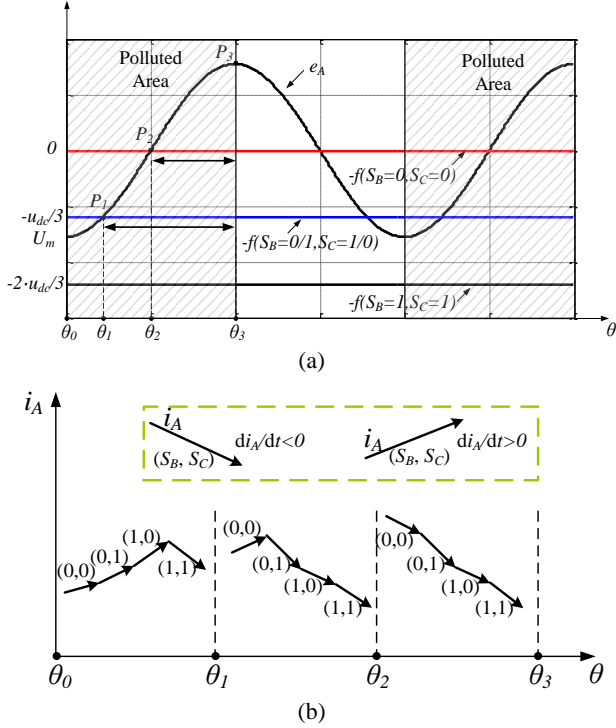


Fig. 6.  $S_{A1}$  OC fault in the capacitive power condition for a two-level SVG: (a) comparison between  $e_A$  and  $-f$ ; (b) effect of  $(S_B, S_C)$  on the sign of  $di_A/dt$ .

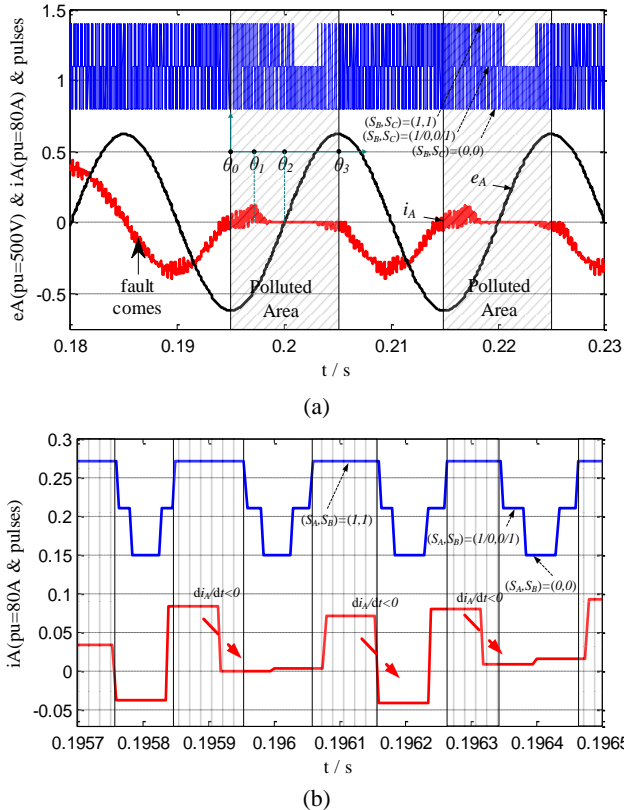


Fig. 7. Simulation results of a  $S_{A1}$  OC fault in the capacitive power condition for a two-level SVG: (a) fault phase current  $i_A$ , supply voltage  $e_A$  and  $(S_B, S_C)$ ; (b)  $di_A/dt$  and  $(S_B, S_C)$ .

### B. Capacitive Reactive Power Condition

When a  $S_{A1}$  OC fault occurs in a two-level SVG in the capacitive reactive power condition, the fault phase current  $i_A$  is still distorted in its positive half cycle, which is also defined as the current-polluted area.

Based on the mathematical models shown in (2)-(5), a comparison of  $e_A$  and  $-f$  is shown in Fig6(a), where  $e_A$  is defined as:

$$e_A = U_m \cdot \sin(\theta - \pi/2) \quad (8)$$

The three intersections of  $e_A$  and  $-f$  in Fig. 6(a) are  $P_1(\theta_1 = \arcsin(-u_{dc}/(3 \cdot U_m)) + 90^\circ)$ ,  $P_2(\theta_2 = 90^\circ)$  and  $P_3(\theta_3 = 180^\circ)$ .

As shown in the interval  $\theta: (\theta_2 - \theta_3)$  in Fig. 6(b),  $di_A/dt < 0$  is true for the values of  $(S_B, S_C)$ , which means that  $i_A$  continues to decrease. Then, Conclusion II is made as follows:

**Conclusion II:** When a  $S_{A1}$  OC fault occurs in a two-level SVG in the capacitive reactive power condition, there must be a zero-current interval with a length of  $90^\circ$ .

Simulation results for this case are illustrated in Fig. 7(a) and Fig. 7(b). The simulation has the same system parameters shown in Table 1. Here,  $(\theta_0, \theta_1, \theta_2, \theta_3)$  are  $(0^\circ, 39.5^\circ, 90^\circ, 180^\circ)$ . Fig. 7(b) shows real time details of  $(S_B, S_C)$  and  $i_A$ , where the value of  $di_A/dt$  changes according to the trend shown in Fig. 6(b).

Simulation results prove that a zero-current interval with a length of  $90^\circ$  must occur when there is a single IGBT OC fault in both the inductive and capacitive reactive power conditions for a two-level SVG. The only difference is that one of the zero-current intervals occurs at the beginning of the current-polluted area, while the other occurs at the end of the current-polluted area.

### III. ZERO-CURRENT ANALYSIS OF AN OC FAULT IN A NPC THREE-LEVEL SVG

The NPC three-level SVG topology is represented in Fig. 8. For each leg (A or B or C), there are 4 IGBTs and 6 Diodes, which are defined as  $S_{X1}, S_{X2}, S_{X3}, S_{X4}, D_{X1}, D_{X2}, D_{X3}, D_{X4}, D_{X1-clamp}$  and  $D_{X2-clamp}$  ( $X \in (A, B, C)$ ). The output current  $i_X$  of leg X is shown in Fig. 8, with a reference direction.

The pulse state is given by:

$$S_X = \begin{cases} 1 & S_{X1} = S_{X2} = on, S_{X3} = S_{X4} = off \\ 0 & S_{X2} = S_{X3} = on, S_{X1} = S_{X4} = off \\ -1 & S_{X3} = S_{X4} = on, S_{X1} = S_{X2} = off \end{cases} \quad (9) \quad (X \in A, B, C)$$

For a three-level SVG, only  $S_{A1}$  and  $S_{A2}$  OC faults are discussed. However, the other 10 IGBT cases can be similarly deduced.

#### A. Inductive Reactive Power Condition

When  $S_{A1}$  experiences an OC fault, if the pulse state  $S_A = 0$  or  $-1$ ,  $S_{A1}$  is not used and is kept off. If  $S_A = 1$  and  $i_X < 0$ , current flows to the dc bus “+” through  $D_{A1}$  and  $D_{A2}$ , and system is

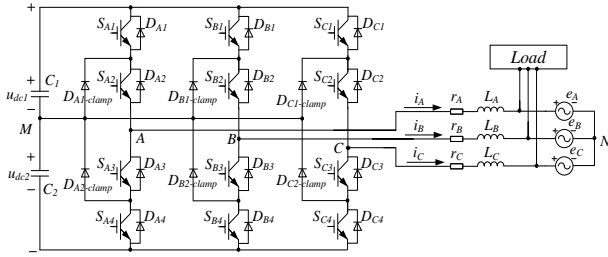
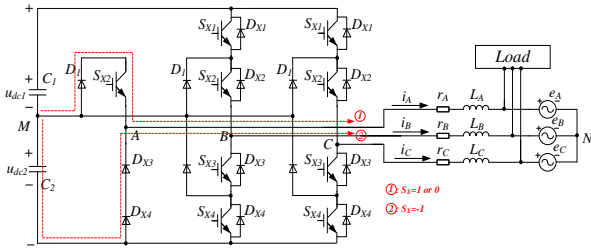


Fig. 8. Schematic of a NPC three-level SVG.

Fig. 9. Simplified schematic of a NPC SVG in the presence of a  $S_{A1}$  OC fault.

not affected. If  $S_A=1$  and  $i_A>0$ , point A is cut off from the dc bus “+” and finds a new current path of  $M \rightarrow D_{A1-clamp} \rightarrow S_{A2} \rightarrow X$ . In this case,  $i_A$  is polluted.

Similarly, the area of  $i_A \geq 0$  is defined as the current-polluted area in the presence of a  $S_{A1}$  OC fault and the system can be simplified as shown in Fig. 9. There are only two possible current paths of  $i_A$  in this case, which are indicated by the dashed lines in Fig. 9.

Assuming that  $u_{dc1}=u_{dc2}=u_{dc}/2$  and ignoring the turn-on voltage drop of the IGBT and diode, the mathematical model of a SVG in the current-polluted area can be expressed as (10)-(13):

$$V_{MN} = \frac{S_A \cdot (S_A - 1)}{2} \cdot \frac{u_{dc}}{2} + i_A \cdot r_A + L_A \cdot \frac{di_A}{dt} + e_A \quad (10)$$

$$V_{MN} = -S_B \cdot \frac{u_{dc}}{2} + i_B \cdot r_B + L_B \cdot \frac{di_B}{dt} + e_B \quad (11)$$

$$V_{MN} = -S_C \cdot \frac{u_{dc}}{2} + i_C \cdot r_C + L_C \cdot \frac{di_C}{dt} + e_C \quad (12)$$

$$i_A \geq 0 \text{ (} S_{A1} \text{ OC fault of three-level SVG)} \quad (13)$$

By (10)-(13), (14) can be easily obtained as follows:

$$-L \cdot \frac{di_A}{dt} = \frac{u_{dc}}{6} \cdot (S_A^2 - S_A + S_B + S_C) + e_A; (i_A \geq 0) \quad (14)$$

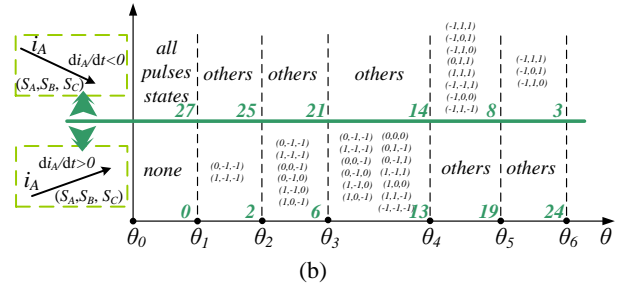
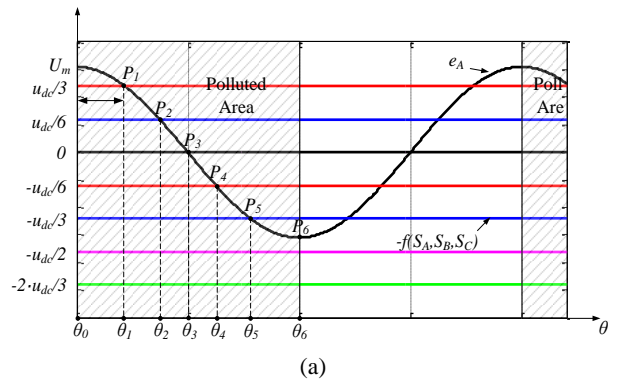
Let  $f = \frac{u_{dc}}{6} \cdot (S_A^2 - S_A + S_B + S_C)$ . Then, all of the possible values of  $-f$  are shown in Table II.

$e_A$  is defined in (7). The curves of  $e_A$  and  $-f$  are shown in Fig. 10(a), with six intersections as follows:  $P_1(\theta_1 = \arccos(u_{dc}/(3 \cdot U_m)))$ ,  $P_2(\theta_2 = \arccos(u_{dc}/(6 \cdot U_m)))$ ,  $P_3(\theta_3 = 90^\circ)$ ,  $P_4(\theta_4 = \arccos(-u_{dc}/(6 \cdot U_m)))$ ,  $P_5(\theta_5 = \arccos(-u_{dc}/(3 \cdot U_m)))$  and  $P_6(\theta_6 = 180^\circ)$ .

Then, the effect of each pulse state  $(S_A, S_B, S_C)$  on the

TABLE II  
VALUES OF  $-f$ 

$(S_A, S_B, S_C)$	$-f$
$(-1, 1, 1)$ ;	$-2 \cdot u_{dc}/3$
$(-1, 0, 1)$ ; $(-1, 1, 0)$ ;	$-u_{dc}/2$
$(0, 1, 1)$ ; $(1, 1, 1)$ ; $(-1, -1, 1)$ ;	$-u_{dc}/3$
$(-1, 0, 0)$ ; $(-1, 1, -1)$ ;	$-u_{dc}/6$
$(0, 0, 1)$ ; $(0, 1, 0)$ ; $(1, 0, 1)$ ;	$-u_{dc}/6$
$(1, 1, 0)$ ; $(-1, -1, 0)$ ; $(-1, 0, -1)$ ;	$-u_{dc}/6$
$(0, 0, 0)$ ; $(0, 1, -1)$ ; $(0, -1, 1)$ ;	0
$(1, -1, 1)$ ; $(1, 0, 0)$ ; $(1, 1, -1)$ ; $(-1, -1, -1)$ ;	0
$(0, 0, -1)$ ; $(0, -1, 0)$ ; $(1, -1, 0)$ ; $(1, 0, -1)$ ;	$u_{dc}/6$
$(0, -1, -1)$ ; $(1, -1, -1)$ ;	$u_{dc}/3$

Fig. 10.  $S_{A1}$  OC fault in the inductive power condition for a NPC three-level SVG: (a) comparison between  $e_A$  and  $-f$ ; (b) effect of  $(S_A, S_B, S_C)$  on the sign of  $di_A/dt$ .

changing rate of  $i_A$  can be determined as shown in Fig. 10(b).

With respect to the 8 pulse vector states of a two-level converter, a three-level converter has 27 pulse vector states, making this case more complicated.

It can be seen that in the interval  $\theta: (\theta_0 - \theta_1)$  of the current-polluted area in Fig. 10(b), for all 27 pulse states,  $di_A/dt < 0$  is true. With the fact that  $i_A$  happens to pass through the zero point at  $\theta_0$ , Conclusion III can be made:

**Conclusion III:** When a  $S_{A1}$  OC fault occurs in a NPC three-level SVG in the inductive reactive power condition, there must be a zero-current interval with a length of  $\theta$ . Here,  $\theta = \arccos(u_{dc}/(3 \cdot U_m))$ .

The corresponding simulation results are shown in Fig. 11. Here, the simulation also shares the system parameters shown



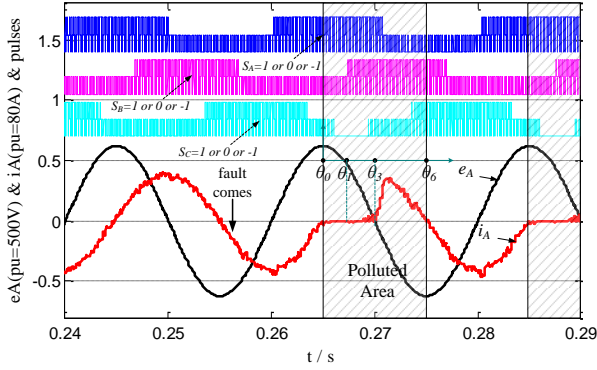


Fig. 11. Simulation results of a  $S_{A1}$  OC fault in the inductive power condition for a NPC three-level SVG .

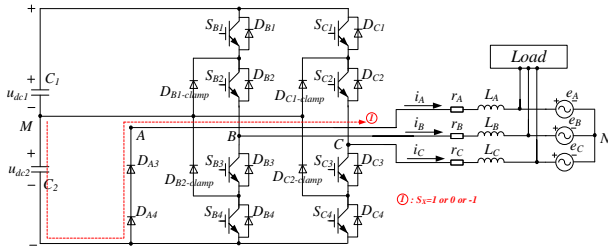


Fig. 12. Simplified schematic of a NPC three-level SVG in the presence of a  $S_{A2}$  OC fault.

in Table I, and  $(\theta_0, \theta_1, \theta_3, \theta_6)$  is  $(0^\circ, 39.5^\circ, 90^\circ, 180^\circ)$ . The value of  $\theta$  mentioned in Conclusion III is  $39.5^\circ$ , corresponding to  $\theta: (\theta_0 - \theta_1)$  in Fig. 11.

Next, a  $S_{A2}$  OC fault will be discussed.

When  $S_{A2}$  experiences an OC fault, if the pulse state  $S_A = -1$ ,  $S_{A2}$  is not used and is kept off. If  $S_A = 0$  and  $i_A < 0$ , current flows to point  $M$  through  $S_{A3}$  and  $D_{A2-clamp}$ , and system is not affected. If  $S_A = 0$  and  $i_A > 0$ , point  $A$  is cut off from point  $M$ , and current flows following the path of “-”  $\rightarrow D_{A4} \rightarrow D_{A3} \rightarrow A$ . In this case,  $i_A$  is polluted. If  $S_A = 1$  and  $i_A < 0$ , current flows to the point “+” through  $D_{A1}$  and  $D_{A2}$ , and system is not affected. If  $S_A = 1$  and  $i_A > 0$ , current flows following the path of “-”  $\rightarrow D_{A4} \rightarrow D_{A3} \rightarrow A$ , and  $i_A$  is polluted.

The area of  $i_A \geq 0$  is defined as the current-polluted area in a  $S_{A2}$  OC fault and the system can be simplified as shown in Fig. 12.

Similarly, the mathematical model of a SVG in the current-polluted area can be expressed as (15)-(18):

$$V_{MN} = \frac{u_{dc}}{2} + i_A \cdot r_A + L_A \cdot \frac{di_A}{dt} + e_A \quad (15)$$

$$V_{MN} = -S_B \cdot \frac{u_{dc}}{2} + i_B \cdot r_B + L_B \cdot \frac{di_B}{dt} + e_B \quad (16)$$

$$V_{MN} = -S_C \cdot \frac{u_{dc}}{2} + i_C \cdot r_C + L_C \cdot \frac{di_C}{dt} + e_C \quad (17)$$

$$i_A \geq 0 \text{ (} S_{A2} \text{ OC fault of three-level SVG)} \quad (18)$$

Then, (19) can be easily obtained as follows:

$$-L \cdot \frac{di_A}{dt} = \frac{u_{dc}}{6} \cdot (2 + S_B + S_C) + e_A \text{ (} i_A \geq 0 \text{)}; \quad (19)$$

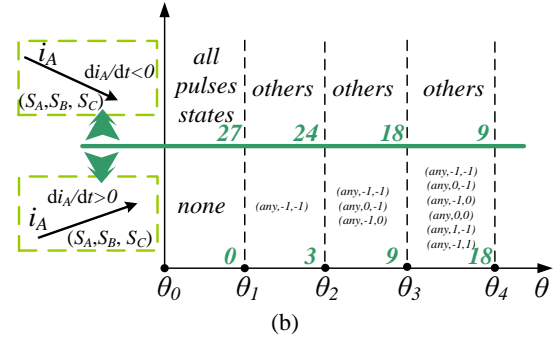
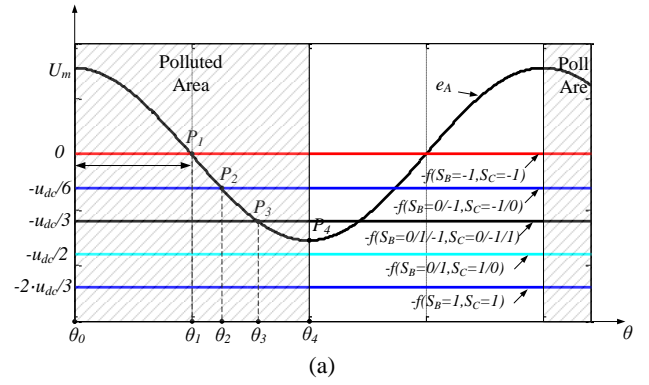


Fig. 13.  $S_{A2}$  OC fault in the inductive power condition for a NPC three-level SVG: (a) comparison between  $e_A$  and  $-f$ ; (b) effects of  $(S_A, S_B, S_C)$  on the sign of  $di_A/dt$ .

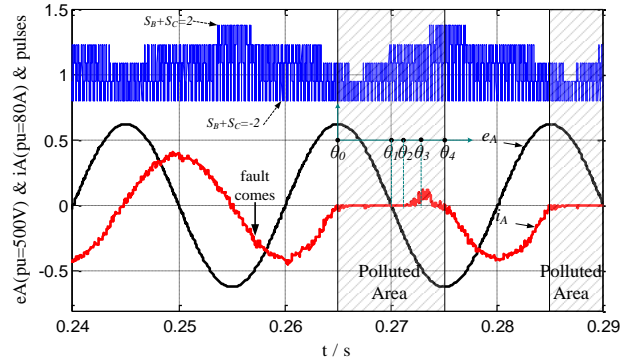


Fig. 14. Simulation results of a  $S_{A2}$  OC fault in the inductive power condition for a NPC three-level SVG.

Let  $f = \frac{u_{dc}}{6} \cdot (2 + S_B + S_C)$ . In addition,  $e_A$  is defined as in

(8). The curves of  $e_A$  and  $-f$  are shown in Fig. 13(a), with four intersections as follows:  $P_1(\theta_1 = 90^\circ)$ ,  $P_2(\theta_2 = \arccos(-u_{dc}/(6 \cdot U_m)))$ ,  $P_3(\arccos(-u_{dc}/(3 \cdot U_m)))$  and  $P_4(\theta_4 = 180^\circ)$ .

When  $S_{A2}$  experiences an OC fault, the effect of each pulse state  $(S_A, S_B, S_C)$  on the sign of the changing rate  $di_A/dt$  can be determined as shown in Fig. 13(b).

In the interval  $\theta: (\theta_0 - \theta_1)$  of the current-polluted area, for all 27 pulse states,  $di_A/dt < 0$  is true. Conclusion IV can be made:

**Conclusion IV:** When a  $S_{A2}$  OC fault occurs in a NPC three-level SVG in the inductive reactive power condition, there must be a zero-current interval with a length of  $90^\circ$ .

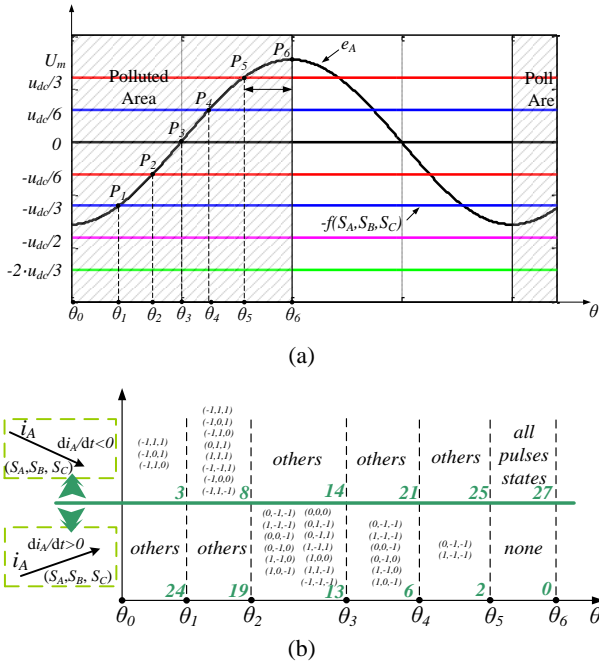


Fig. 15.  $S_{A1}$  OC fault in the capacitive power condition for a NPC three-level SVG: (a) comparison between  $e_A$  and  $-f$ ; (b) effect of  $(S_A, S_B, S_C)$  on the sign of  $di_A/dt$ .

Simulation results of a  $S_{A2}$  OC fault are shown in Fig. 14, where the zero-current interval corresponds to  $\theta: (\theta_0 - \theta_1)$ . Here,  $(\theta_0, \theta_1, \theta_2, \theta_3, \theta_4)$  are  $(0^\circ, 90^\circ, 112.7^\circ, 140.5^\circ, 180^\circ)$ .

It can be seen from a comparison between Fig. 14 and Fig. 11 that a  $S_{A2}$  OC fault has a greater influence on the system than a  $S_{A1}$  OC fault.

### B. Capacitive Reactive Power Condition

When capacitive reactive power is generated in a NPC three-level SVG, the interval-current interval can be similarly deduced.

First, if  $S_{A1}$  experiences an open circuit fault,  $e_A$  in (7) and  $-f$  in (14) are drawn in Fig. 15(a), with six intersections as follows:  $P_1(\theta_1 = \arcsin(-u_{dc}/(3 \cdot U_m)) + 90^\circ)$ ,  $P_2(\theta_2 = \arcsin(-u_{dc}/(6 \cdot U_m)) + 90^\circ)$ ,  $P_3(\theta_3 = 90^\circ)$ ,  $P_4(\theta_4 = \arcsin(u_{dc}/(6 \cdot U_m)) + 90^\circ)$ ,  $P_5(\theta_5 = \arcsin(u_{dc}/(3 \cdot U_m)) + 90^\circ)$  and  $P_6(\theta_6 = 180^\circ)$ .

Then the effect of each pulse state  $(S_A, S_B, S_C)$  on the rate of the current  $i_A$  can be determined as shown in Fig. 15(b).

Similarly, Conclusion V is drawn:

**Conclusion V:** When a  $S_{A1}$  OC fault occurs in a NPC three-level SVG in the capacitive reactive power condition, there must be a zero-current interval with a length of  $\theta$ . Here,  $\theta = \arcsin(u_{dc}/(3 \cdot U_m))$ .

When compared with the inductive power condition, the zero-current interval comes at the end of the current-polluted area, which corresponds to  $\theta: (\theta_5 - \theta_6)$  in the simulation results presented in Fig. 16.

Next, a  $S_{A2}$  OC fault will be discussed.

If  $S_{A2}$  experiences an open circuit fault,  $e_A$  in (8) and  $-f$  in (19)

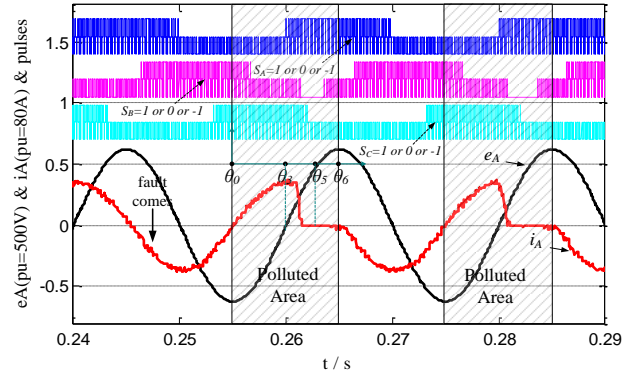


Fig. 16. Simulation results of a  $S_{A1}$  OC fault in the capacitive power condition for a NPC three-level SVG.

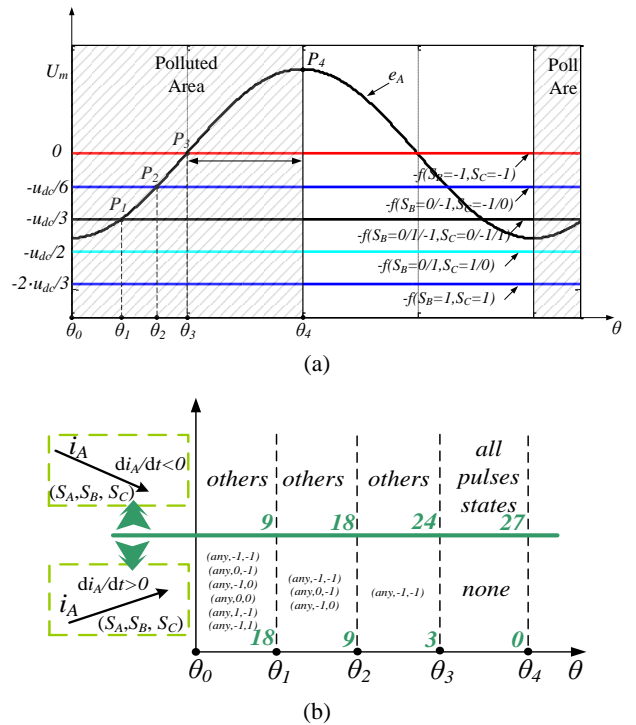


Fig. 17.  $S_{A2}$  OC fault in the capacitive power condition for a NPC three-level SVG: (a) comparison between  $e_A$  and  $-f$ ; (b) effect of  $(S_A, S_B, S_C)$  on the sign of  $di_A/dt$ .

are drawn in Fig. 17(a), with four intersections as follows:  $P_1(\theta_1 = \arcsin(-u_{dc}/(3 \cdot U_m)) + 90^\circ)$ ,  $P_2(\theta_2 = \arcsin(-u_{dc}/(6 \cdot U_m)) + 90^\circ)$ ,  $P_3(\theta_3 = 90^\circ)$  and  $P_4(\theta_4 = 180^\circ)$ .

The effect of each pulse state  $(S_A, S_B, S_C)$  on the rate of the current  $i_A$  can be determined as shown in Fig. 17(b).

Noticing that in the interval  $\theta: (\theta_3 - \theta_4)$ ,  $di_A/dt < 0$  is true for all 27 pulse states, Conclusion VI is made:

**Conclusion VI:** When a  $S_{A2}$  OC fault occurs in a NPC three-level SVG in the capacitive reactive power condition, there must be a zero-current interval with a length of  $90^\circ$ .

Simulation results for this case are shown in Fig. 18, where the zero-current interval corresponds to  $\theta: (\theta_3 - \theta_4)$ .

In summary, Table III shows the length of the zero-current



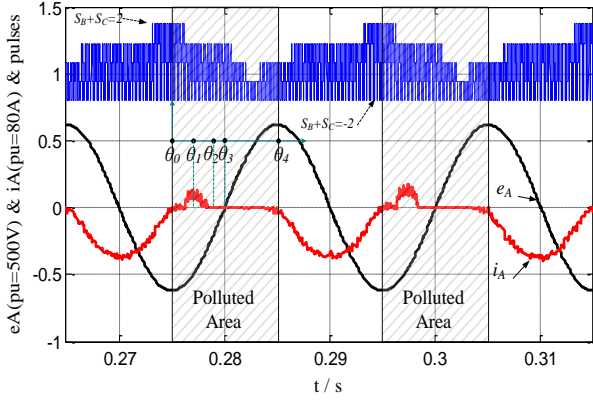


Fig. 18. Simulation results of a  $S_{A2}$  OC fault in the capacitive power condition for a NPC three-level SVG.

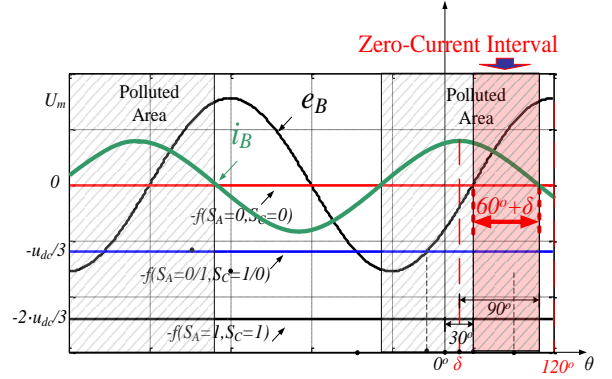


Fig. 19. Zero current interval in the unbalanced condition for a two-level SVG.

TABLE III  
SUMMARY OF THE ZERO-CURRENT INTERVAL FOR ALL CASES

Topology	Fault Location	Length of Zero-Current Interval for both Inductive and Capacitive Power Condition
	$S_{X1}$	$90^\circ$ (1/4 of supply period)
	$S_{X2}$	
	$S_{X1}$	$\arccos(u_{dc}/(3 \cdot U_m))$
	$S_{X2}$	
	$S_{X3}$	$90^\circ$ (1/4 of supply period)
	$S_{X4}$	

interval for all single IGBT OC faults. For both inductive and capacitive reactive power conditions, the zero current intervals share the same length. However, they occur at different times which are determined by the phase of the voltage and current.

#### IV. UNBALANCED LOAD AND INPUT VOLTAGE CASES DISCUSSION

In the unbalanced load situation, the three phase currents can be decomposed into positive sequence current  $I_m^+$ , negative sequence current  $I_m^-$  and zero sequence current  $I_m^0$ . For a three wire system, only positive sequence and negative sequence currents exist. Assuming that  $e_A = U_m \cos(\theta)$ ,  $e_B = U_m \cos(\theta - 120^\circ)$  and  $e_C = U_m \cos(\theta + 120^\circ)$ , the three phase currents in the normal condition are:

$$\begin{cases} i_A = i_A^+ + i_A^- = I_m^+ \cos(\theta + \theta^+) + I_m^- \cos(\theta + \theta^-) \\ i_B = i_B^+ + i_B^- = I_m^+ \cos(\theta + \theta^+ - 120^\circ) + I_m^- \cos(\theta + \theta^- + 120^\circ) \\ i_C = i_C^+ + i_C^- = I_m^+ \cos(\theta + \theta^+ + 120^\circ) + I_m^- \cos(\theta + \theta^- - 120^\circ) \end{cases} \quad (20)$$

Where  $\theta^{\pm}$  represents the angle between the positive/negative sequence current and the input voltage of phase A.

For example, if a  $S_{B1}$  OC fault occurs in phase  $B$  of a two-level SVG, then  $i_B$  can be expressed by:

$$i_B = I_m^+ \cos(\theta - \delta). \quad (21)$$

Where  $\delta = \arccos\left(\frac{I_m^+ \cos(\theta^+ - 120^\circ) + I_m^- \cos(\theta^+ + 120^\circ)}{\sqrt{(I_m^+ \cos(\theta^+ - 120^\circ) + I_m^- \cos(\theta^+ + 120^\circ))^2 + (I_m^+ \sin(\theta^+ - 120^\circ) - I_m^- \sin(\theta^+ + 120^\circ))^2}}\right)$ . Then,

the zero current interval of a  $S_{B1}$  OC fault in the unbalanced load condition for a two-level SVG is shown in Fig. 19.

Therefore, when negative sequence currents are involved, the zero current interval is decided by  $\delta$ . Here,  $(120^\circ - \delta)$  is the angle between  $e_X$  and  $i_X$ . For a two-level SVG, the absolute length of the zero current interval of an OC fault is  $(60^\circ + \delta)$ . For a three-level SVG, the zero current interval can be obtained through the same analysis method, which is similar to the above conclusion and not discussed here.

Unbalanced load currents at the same time lead to input voltage unbalance, which is caused by the voltage drop on the line impedance and equivalent impedance of the transformer. In this case, the zero current interval is effected by both the phase deviation of the input voltage  $e_X$  (caused by a negative sequence voltage injection) and  $\delta$ . However, the expression of the unbalanced input voltage is too complicated to deduce. For the light unbalanced input voltage condition, the zero current interval is mainly decided by  $\delta$ .

#### V. EXPERIMENTAL VERIFICATION

First, a two-level SVG prototype, shown in Fig. 20(a), is developed to verify Conclusions I and II. Then, a three-level NPC prototype, shown in Fig. 20(b), is developed to verify Conclusions III to VI.

The experimental parameters are listed in Table IV.

For both the two-level and three-level SVGs, two typical reactive powers, inductive reactive powers and capacitive reactive powers, are generated to show whether the open-circuit fault current is bound to have a zero-current interval as described in Conclusions I through VI. An OC

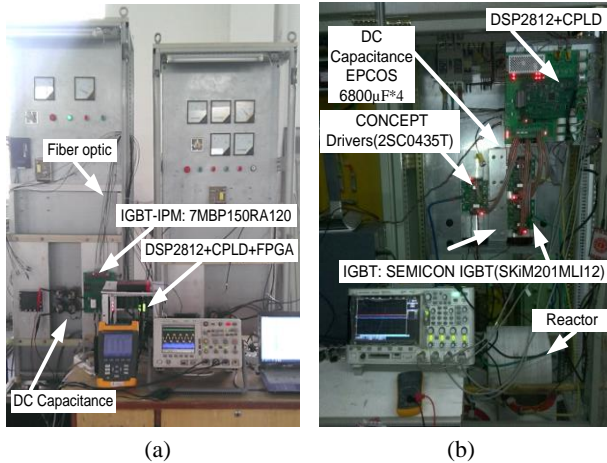


Fig. 20. Experimental prototypes: (a) two-level; (b) NPC three-level.

TABLE IV  
EXPERIMENTAL PARAMETERS

	Parameters	Values
<b>Two-level</b>	$e_{AB}, e_{BC}, e_{CA}$	380V(RMS)
	$i_A, i_B, i_C$	18A(RMS)
	$L_A, L_B, L_C$	1.5mH
	$u_{dc}$	720V
	Bus capacitance $C$	2200µF
	Switching frequency	2.5kHz
	Sampling frequency	12.5kHz
<b>NPC Three-level</b>	$e_{AB}, e_{BC}, e_{CA}$	380V(RMS)
	$i_A, i_B, i_C$	14A(RMS)
	$L_A, L_B, L_C$	2mH
	$u_{dc}$	720V
	Bus capacitance $C$	6800µF
	Switching frequency	5kHz
	Sampling frequency	10kHz

fault is achieved by unplugging the fiber pulse or by blocking the pulses in the CPLD control unit.

In fact, when the OC fault occurs, the three-phase current is distorted. Here, the focus is on the fault phase current changes, since it is of great regularity.

Experimental results of the two-level SVG are shown in Fig. 21. In Fig. 21(a), an OC fault occurs in the inductive reactive power condition and at the beginning of each positive half-cycle of the fault-phase current, i.e. the current-polluted area. In addition, a zero-current interval of 90 degrees appears, as described in Conclusion I. In Fig. 21(b), an OC fault occurs in

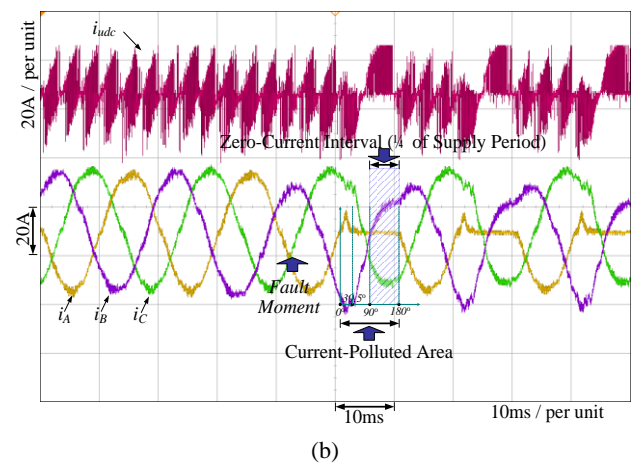
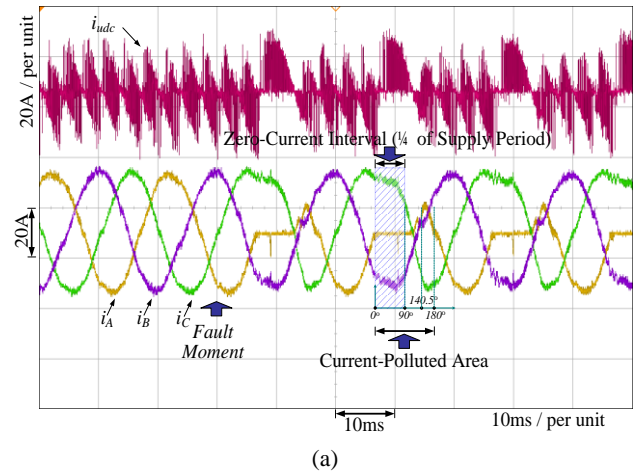


Fig. 21.  $S_{A1}$  OC fault for a two-level SVG: (a) inductive reactive power condition; (b) capacitive reactive power condition.

the capacitive reactive power condition and at the end of each positive half-cycle of the fault-phase current, i.e. the current-polluted area. In addition, a zero-current interval of 90 degrees appears, as described in Conclusion II.

Next, experimental results of a NPC three-level SVG are illustrated in Fig. 22.

As shown in Fig. 22, for a three-level SVG, a  $S_{A2}$  OC fault has a more severe impact on the system than a  $S_{A1}$  OC fault. Consistent with conclusions III to VI, a 90 degree zero-current interval appears in the  $S_{A2}$  OC fault, while a 39.5 degree zero-current interval appears in the  $S_{A1}$  OC fault.

It is worth emphasizing that Conclusions I through VI are independent of the system parameters. As long as the system is running under the pure inductive or capacitive reactive power case, the fault phase current must have a corresponding length of the zero-current interval.

Due to Conclusions I through VI, there is a better understanding of the effects of OC faults on the fault phase current. This is instructive for future OC fault location studies.

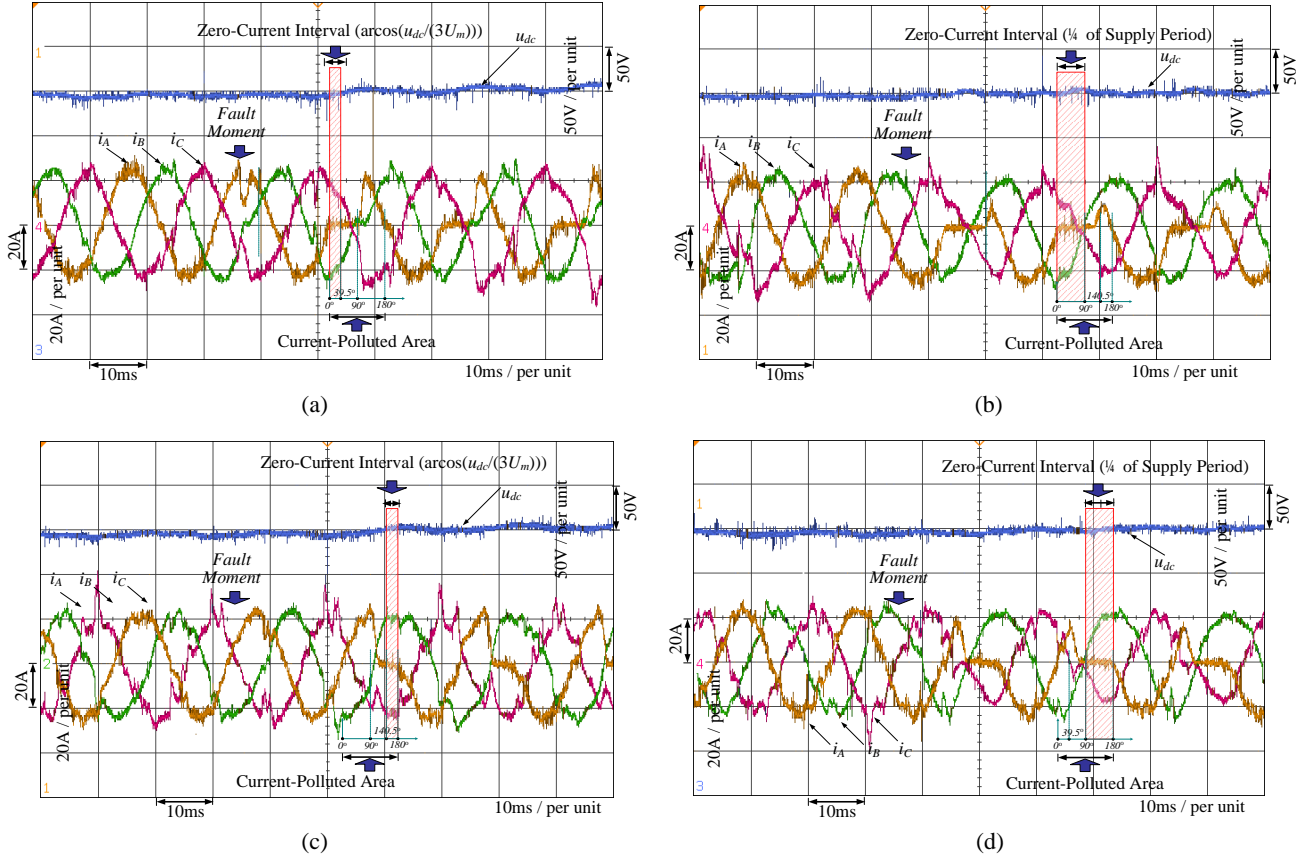


Fig. 22. OC fault for a two-level SVG: (a)  $S_{A1}$  OC fault for the inductive reactive power condition; (b)  $S_{A2}$  OC fault for the inductive reactive power condition; (c)  $S_{A1}$  OC fault for the capacitive reactive power condition; (d)  $S_{A2}$  OC fault for the capacitive reactive power condition.

## VI. CONCLUSIONS

When a single IGBT OC fault occurs in two-level and NPC three-level converters, the three-phase currents are distorted, especially the fault phase current which can drop directly to zero in some cases. A method to effectively analyze the changing rules of fault current has not been discussed in previous studies. In this paper, an effective method based on learning the current change rate is proposed to summarize the rules of fault phase current. Taking a SVG as the research object, a mathematical model under an OC fault is introduced. Then, the influence of the pulse on the sign of the current changing rate is analyzed. Finally, some conclusions are drawn. A zero-current interval with a length of  $1/4$  of a supply period follows the OC fault in both pure inductive and capacitive reactive power conditions for a two-level SVG. On the other hand, for a three-level SVG, a zero-current interval with length of  $\arcsin(u_{dc}/(3 \cdot U_m))$  follows  $S_{X1}$  and  $S_{X4}$  OC faults and a zero-current interval with a length of  $1/4$  of a supply period follows  $S_{X2}$  and  $S_{X3}$  OC faults. The theoretical analysis and conclusions are instructive for future OC fault location studies.

## ACKNOWLEDGMENT

The work described in this paper was fully supported by

Special Fund for the Transformation of Scientific and Technological Achievements of Jiangsu Province (No. BA2016017), and Sub Project of the National Key R & D Program (No. 2016YFC0600804).

## REFERENCES

- [1] Y. Shaoyong, A. Bryant, P. Mawby, D. Xiang, L. Ran, and P. Tavner, "An industry-based survey of reliability in power electronic converters," *IEEE Trans. Ind. Appl.*, Vol. 47, No. 3, pp. 1441-1451, May/June 2011.
- [2] S. Ouni, M. R. Zolghadri, J. Rodriguez, M. Shahbazi, H. Oraee, P. Lezana, and A. U. Schmeisser, "Quick diagnosis of short circuit faults in cascaded h-bridge multilevel inverters using FPGA," *J. Power Electron.*, Vol. 17, No. 1, pp. 56-66, Jan. 2017.
- [3] L. Bin and S. K. Sharma, "A literature review of IGBT fault diagnostic and protection methods for power inverters," *IEEE Trans. Ind. Appl.*, Vol. 45, No. 5, pp. 1770-1777, Sep./Oct. 2009.
- [4] B. Mirafzal, "Survey of fault-tolerance techniques for three-phase voltage source inverters," *IEEE Trans. Ind. Electron.*, Vol. 61, No. 10, pp. 5192-5202, Oct. 2014.
- [5] A. M. S. Mendes, A. J. M. Cardoso, and E. S. Saraiva, "Voltage source inverter fault diagnosis in variable speed ac drives, by Park's vector approach," in *Proc. 7th Int. Conf. Power Electron. Variable Speed Drives (456)*, pp.

- 538-543, 1998.
- [6] J. O. Estima, N. M. A. Freire, and A. J. M. Cardoso, "Recent advances in fault diagnosis by Park's vector approach," in *Proc. IEEE WEMDCD*, pp. 279-288, 2013.
- [7] J. A. A. Caseiro, A.M. S.Mendes, and A. J.M. Cardoso, "Open-Circuit Fault Diagnosis and Fault-Tolerant Control for a Grid-Connected NPC Inverter tolerance using the average current Park's Vector approach," in *Proc. IEEE IEMDC, Miami, FL, USA, 2009*, pp. 695-701, 2009.
- [8] R. Peugot, S. Courtine, and J. P. Rognon, "Fault detection and isolation on a PWM inverter by knowledge-based model," *IEEE Trans. Ind. Appl.*, Vol. 34, No. 6, pp. 1318-1326, Nov./Dec. 1998.
- [9] M. Trabelsi, M. Boussak, and M. Gossa, "Multiple IGBTs open circuit faults diagnosis in voltage source inverter fed induction motor using modified slope method," in *Proc. XIX Int. Conf. Electr. Mach.*, pp. 1-6, 2010.
- [10] W. Sleszynski, J. Nieznanski, and A. Cichowski, "Open-transistor fault diagnostics in voltage-source inverters by analyzing the load currents," *IEEE Trans. Ind. Electron.*, Vol. 56, No. 11, pp. 4681-4688, Nov. 2009.
- [11] J. O. Estima and A. J.M. Cardoso, "A new approach for real-time multiple open-circuit fault diagnosis in voltage source inverters," *IEEE Trans. Ind. Appl.*, Vol. 47, No. 6, pp. 2487-2494, Nov./Dec. 2011.
- [12] N. M. A. Freire, J. O. Estima, and A. J. M. Cardoso, "Multiple open-circuit fault diagnosis in voltage-fed PWM motor drives using the current Park's vector phase and the currents polarity," in *Proc. 8th IEEE Int. Symp. Diagnost. Elect. Mach., Power Electron. Drives*, pp. 397-404., 2011.
- [13] N. M. A. Freire, J. O. Estima, and A. J. M. Cardoso, "A voltage-based approach without extra hardware for open-circuit fault diagnosis in closed-loop PWM AC regenerative drives," *IEEE Trans. Ind. Electron.*, Vol. 61, No. 9, pp. 4960-4970, Sep. 2014.
- [14] M. Shahbazi, P. Poure, S. Saadate, and M. R. Zolghadri, "FPGA-based fast detection with reduced sensor count for a fault-tolerant three-phase converter," *IEEE Trans. Ind. Informat.*, Vol. 9, No. 3, pp. 1343-1350, Aug. 2013.
- [15] R. Ribeiro, C. Jacobina, E. da Silva, and A. Lima, "Fault detection of open-switch damage in voltage-fed PWM motor drive systems," *IEEE Trans. Power Electron.*, Vol. 18, No. 2, pp. 587-593, Mar. 2003.
- [16] S. Karimi, A. Gaillard, P. Poure, and S. Saadate, "FPGA-based real-time power converter failure diagnosis for wind energy conversion systems," *IEEE Trans. Ind. Electron.*, Vol. 55, No. 12, pp. 4299-4308, Dec. 2008.
- [17] Q.-T. An, L.-Z. Sun, K. Zhao, and L. Sun, "Switching function model-based fast-diagnostic method of open-switch faults in inverters without sensors," *IEEE Trans. Power Electron.*, Vol. 26, No. 1, pp. 119-126, Jan. 2011.
- [18] M. R. Mamat, M. Rizon, and M. S. Khanniche, "Fault detection of 3-phase VSI using wavelet-fuzzy algorithm," *Amer. J. Appl. Sci.*, Vol.3, No. 1, pp. 1642-1648, Mar. 2006.
- [19] F. Charfi, F. Sellami, and K. Al-Haddad, "Fault diagnosis in power system using wavelet transforms and neural networks," in *Proc. IEEE Int. Symp. Ind. Electron.*, pp. 1143-1148, 2006.
- [20] K. Debebe, V. Rajagopalan, and T. S. Sankar, "Expert systems for fault diagnosis of VSI fed ac drives," in *Conf. Rec. IEEE IAS Annu. Meeting*, pp. 368-373, 1991.
- [21] U. Choi, K. Lee, and F. Blaabjerg, "Diagnosis and tolerant strategy of an open-switch fault for t-type three-level inverter systems," *IEEE Trans. Ind. Appl.*, Vol. 50, No. 1, pp. 495-508, Jan./Feb. 2014.
- [22] A. Mohammadpour, S. Sadeghi, and L. Parsa, "A generalized fault-tolerant control strategy for five-phase PM motor drives considering star, pentagon, and pentacle connections of stator windings," *IEEE Trans. Ind. Electron.*, Vol. 61, No. 1, pp. 63-75, Jan. 2014.
- [23] A. L. Julian and G. Oriti, "A comparison of redundant inverter topologies to improve voltage source inverter reliability," *IEEE Trans. Ind. Appl.*, Vol. 43, No. 5, pp. 1371-1378, Sep./Oct. 2007.
- [24] S. Ceballos, J. Pou, J. Zaragoza, E. Robles, J. L. Villate, and J. L. Martin, "Fault-tolerant neutral-point-clamped converter solutions based on including a fourth resonant leg," *IEEE Trans. Ind. Electron.*, Vol. 58, No. 6, pp. 2293-2303, Jun. 2011.
- [25] M. B. Abadi, A. M. S. Mendes, S. M. A. Cruz, "Three-level NPC inverter fault diagnosis by the average current Park's vector approach," *2012 International Conference on Electrical Machines*, pp. 1893-1898, 2012.
- [26] U.-M. Choi, H.-G. Jeong, K.-B. Lee, and F. Blaabjerg, "Method for detecting an open-switch fault in a grid-connected NPC inverter system," *IEEE Trans. Power Electron.*, Vol. 27, No. 6, pp. 2726-2739, Jun. 2012.
- [27] S.-M. Jung, J.-S. Park, H.-W. Kim, K.-Y. Cho, and M.-J. Youn, "An MRAS-based diagnosis of open-circuit fault in PWM voltage-source inverters for PM synchronous motor drive systems," *IEEE Trans. Power Electron.*, Vol. 28, No. 5, May 2013.
- [28] A. M. S. Mendes, M. B. Abadi, and S. M. A. Cruz, "Fault diagnostic algorithm for three-level neutral point clamped AC motor drives, based on the average current Park's vector," *IET Power Electron.*, Vol. 7, No. 5, pp. 1127-1137, May 2014.
- [29] J. O. Estima and A. J. M. Cardoso, "A new algorithm for real-time multiple open-circuit fault diagnosis in voltage-fed PWM motor drives by the reference current errors," *IEEE Trans. Ind. Electron.*, Vol. 60, No. 8, pp. 3496-3505, Aug. 2013.
- [30] Q.-T. An, L.-Z. Sun, K. Zhao, and L. Sun, "Switching function model-based fast-diagnostic method of open-switch faults in inverters without sensors," *IEEE Trans. Power Electron.*, Vol. 26, No. 1, pp. 119-126, Jan. 2011.
- [31] L. Tian, F. Wu, Y. Shi, and J. Zhao, "A current dynamic analysis based open-circuit fault diagnosis method in voltage-source inverter fed induction motors," *J. Power Electron.*, Vol. 17, No. 3, pp. 725-732, May 2017.
- [32] C. Shu, C. Ya-Ting, Y. Tian-Jian, and W. Xun, "A novel diagnostic technique for open-circuited faults of inverters based on output line-to-line voltage model," *IEEE Trans. Ind. Electron.*, Vol. 63, No. 7, pp. 4412-4421, Feb. 2016.
- [33] M. B. Abadi, A. M. S. Mendes, and S. M. A. Cruz, "A real-time method for the diagnosis of multiple switch faults in NPC inverters based on output currents analysis," *J. Power Electron.*, Vol. 16, No. 4, pp. 1415-1425, Jul. 2016.
- [34] U.-M. Choi, K.-B. Lee, and F. Blaabjerg, "Diagnosis and tolerant strategy of an open-switch fault for T-type three-level inverter systems," *IEEE Trans. Ind. Appl.*, Vol. 50, No. 1, pp. 495-508, Jan./Feb. 2014.
- [35] J. Li, A. Q. Huang, Z. Liang, and S. Bhattacharya, "Analysis and design of active NPC (ANPC) inverters for fault-tolerant operation of high-power electrical drives," *IEEE Trans. Power Electron.*, Vol. 27, No. 2, pp. 519-533,



Feb. 2012.

- [36] U.-M. Choi, J.-S. Lee, F. Blaabjerg, and K.-B. Lee, "Open-circuit fault diagnosis and fault-tolerant control for a grid-connected NPC inverter," *IEEE Trans. Power Electron.*, Vol. 31, No. 10, pp. 7234-7247, Oct. 2016.
- [37] D.-K. Choi, S.-H. Moon, and K.-B. Lee, "An open-switch fault detection method and tolerance controls based on MPDPC in a NPC rectifier," in *Proc. IEEE CENCON*, pp. 354-359, 2014.
- [38] L. M. A. Caseiro, A. M. S. Mendes, P. M. A. F. Lopes, "Open-circuit fault diagnosis in neutral-point-clamped active power filters based on instant voltage error with no additional sensors," *2015 IEEE Applied Power Electronics Conference and Exposition*, pp. 2217-2222, 2015.
- [39] U.-M. Choi, H.-G. Jeong, K.-B. Lee, and F. Blaabjerg, "Method for detecting an open-switch fault in a grid-connected NPC inverter system," *IEEE Trans. Power Electron.*, Vol. 27, No. 6, pp. 2726-2739, Jun. 2012.
- [40] E. R. da Silva, W. S. Lima, A. S. de Oliveira, C. B. Jacobina, and H. Razik, "Detection and compensation of switch faults in a three level inverter," *2006 37th IEEE Power Electronics Specialists Conference*, pp. 1-7, 2006.



**Ke Wang** was born in Xuzhou, China, in 1985. He received his B.S. degree in Electrical Engineering and Automation, and his M.S. degree in Power Electronics and Drives from the China University of Mining and Technology, Xuzhou, China, in 2005 and 2009, respectively, where he is presently working towards his Ph.D. degree in the School of Electrical and Power Engineering. His current research interests include power quality compensation systems, fault diagnosis and power electronics.



**Hong-Lu Zhao** was born in Xuzhou, China, in 1994. She received her B.S. degree from the Zhejiang Sci-Tech University, Hangzhou, China, in 2016. She is presently working towards her M.S. degree at the China University of Mining and Technology, Xuzhou, China. Her current research interests include thermal characterization modeling of IGBT power modules and the fault-tolerant control of inverters.



**Yi Tang** was born in Zhangjiagang, China, in 1957. He received his Ph.D. degree from the School of Information and Electrical Engineering, China University of Mining and Technology, Xuzhou, China, in 1995. He is presently working as a Professor in the China University of Mining and Technology. His current research interests include power quality and power system analysis.



**Xiao Zhang** was born in Baoji, China, in 1974. He received his M.S. and Ph.D. degrees from the School of Information and Electrical Engineering, China University of Mining and Technology, Xuzhou, China, in 2003 and 2012, respectively. In 1997, he joined the China University of Mining and Technology as a Teaching Assistant, where he has been an Associate Professor since 2009. From October 2013 to October 2014, he was a Visiting Professor at Ohio State University, Columbus, OH, USA. His current research interests include power electronic converters, reactive power control, harmonics, power quality compensation systems, and the application of power electronics in renewable energy systems and motor control.



**Chuan-Jin Zhang** was born in Xuzhou, China, in 1986. He received his B.S. degree from the School of Electrical Engineering, Northeast Dianli University, Jilin, China, in 2009; and his M.S. degree in Power Electronics and Drives from the China University of Mining and Technology, Xuzhou, China, in 2012, where he is presently working towards his Ph.D. degree in the School of Electrical and Power Engineering. His current research interests include power quality compensation systems, motor control and power electronics.